



rozšíření píků a určit jednoznačně rozdělení velikosti krystalitů. Překvapivá je přítomnost velké mikrodeformace uvnitř krystalitů (velká hustota dislokací - asi  $6 \times 10^{15} \text{ m}^{-2}$ ) a výskyt růstových vrstevných poruch (až 8% ve vzorku s nejmenšími částicemi).

- [1] M. Šlouf, R. Kužel, Z. Matěj, *Materials Structure*, **11** (2004) 166-168.  
 [2] M. Šlouf, přednáška na tomto kolokviu.  
 [3] B. E. Warren: *X-ray diffraction*. 1969. Addison-Wesley.  
 [4] V. Valvoda a kolektiv: *Základy strukturní analýzy*. Praha 1992. Karolinum.  
 [5] M. A. Krivoglaz: *X-ray and Neutron Diffraction in Nonideal Crystals*. Berlin 1996. Springer-Verlag.  
 [6] P. Scardi, M. Leoni, *Acta Cryst. A*, **58** (2002) 190-200.  
 [7] P. Scardi, M. Leoni, Y. H. Dong, *Eur. Phys. J. B*, **18** (2000) 23-30.  
 [8] T. Ungár, I. Dragomir-Cernatescu, D. Louer, N. Audebrand, *J. Phys. Chem. Sol.*, **62** (2001) 1935-1941.

**Tabulka 1.** Teoretická velikost zrn ( $d_{\text{theor}}$ ), velikost krystalitů určená z rozšíření profilů ( $d_{\text{diff}}$ ), hustota dislokací ( $\rho_{\text{diff}}$ ) a pravděpodobnost výskytu růstových vrstevných chyb ( $b_{\text{twin}}$ ) určené z rtg. difrakčních profilů.

|     | $d_{\text{theor}}$<br>(nm) | $d_{\text{diff}}$<br>(nm) | $\rho_{\text{diff}}$<br>(10 <sup>6</sup> m <sup>-2</sup> ) | $b_{\text{twin}}$ |
|-----|----------------------------|---------------------------|--|-------------------|
| Au1 | 4.5                        | 10±6                      | 5±2  | 0.08±0.03         |
| Au2 | 11.1                       | 15±5                      | 6±1  | 0.07±0.02         |
| Au3 | 33.4                       | 31±5                      | 6.6±0.5  | 0.05±0.01         |
| Au4 | 101.5                      | 92±20                     | 9±2  | 0.012<br>±0.005   |

- [9] A. Borbély, J. Dragomir-Cernatescu, G. Ribárik, T. Ungár, *J. Appl. Cryst.*, **36** (2003) 160-162.  
 [10] P. Scardi, M. Leoni, R. Delhez, *J. Appl. Cryst.*, **37** (2004) 381-390.

S15

## STRUCTURE OF FC-FRAGMENT OF THE MOUSE IMMUNOGLOBULIN

Petr Kolenko<sup>1,3</sup>, Jan Dohnálek<sup>1</sup>, Renata Štouračová<sup>2</sup>, Tereza Skálová<sup>1</sup>, Galina Tiščenko<sup>1</sup>, Jarmila Dušková<sup>1</sup>, Jindřich Hašek<sup>1</sup>, hasek@imc.cas.cz

<sup>1</sup>Institute of Macromolecular Chemistry, Academy of Sciences of CR,

<sup>2</sup>Institute of Molecular Genetics, Academy of Sciences of CR

<sup>3</sup>Faculty of Nuclear Sciences and Physical Eng., Czech Technical University of Prague

Immunoglobulines play an irreplaceable role in the immunity system in all higher organisms. Because of its role in activation of immunological reaction against infected cells, immunoglobulines are routinely used in medical applications. There is a very reliable way of IgG purification based on its affinity to the B fragment of the protein A from *Staphylococcus Aureus*. However, the costs of production of protein A are significant and thus a new method of rapid and cheap production of purified immunoglobulines in non-denaturing conditions is worth of our special interest. Any highly selective separation process should be based on molecular recognition between a specially designed ligand and the immunoglobulin surface.

In spite of an immense diversity of Fab fragments containing the hypervariable regions (responsible for molecular recognition of antibody) at the antigen binding sites, the immunoglobulines of the same type (e.g. IgG2b) share very similar aminoacid sequences of Fc fragment. The object of our interest is Fc-fragment, because of its invariant structure. Explication of structure of this fragment and its interaction with other molecules can help in design of polymer sorbents for affinity chromatography.

### Structure determination

Monoclonal antibody, class IgG2b was cleaved by papain and purified in 4C on BioLOGIC LP System (BIORAD) using protein A Sepharose column (Biorad). The measured crystal was grown under the following conditions:

**Reservoir:** HEPES pH 7.5, PEG 2000 20 % (w/v).

**Drop:** 1  $\mu$ l of reservoir solution plus 1  $\mu$ l of protein 8 mg/ml, PBS (phosphate buffer saline) pH 7.5.

**Cryoprotectant:** 20 % glycerol.

The diffracted intensities (total 34029 independent reflections) was collected at the ID-29 beamline at the synchrotron ESRF in Grenoble with the diffraction limit 2.2 Å. The measured crystal (a triangle platelet 0.3 × 0.02 mm) was flash cooled to 100 K. Space group is C2, the unit cell  $a = 135,73 \text{ Å}$ ,  $b = 62,75 \text{ Å}$ ,  $c = 69,81 \text{ Å}$ ,  $\beta = 103,35^\circ$ . Data reduction was performed by program package HKL (Denzo, Scalepack, Xdisp) [1]. The phase problem was solved by molecular replacement (program AMORE [2]) using the structure model 1IGT taken from PDB [7] (sequence similarity 79 %). The other data processing was done mostly using the program package CCP4 [3]. The structure refinement was done by program REFMAC [4]. Manual corrections were done by program XtalView [5], the solvent water molecules determined with help of ARP/wARP [6]. The methods used were similar as described in [9]. The final R factors are  $R = 0.19$ ,  $R_{\text{free}} = 0.25$ . The refined structure satisfies all criteria set by program Procheck [7].

Both protein chains of the Fc fragment IgG2b (residues from Gly125A to Arg331A and Gly125B to Arg331B) were uniquely identified in the maps of electron density (except of conformational alternatives evident at side chains of several residues).

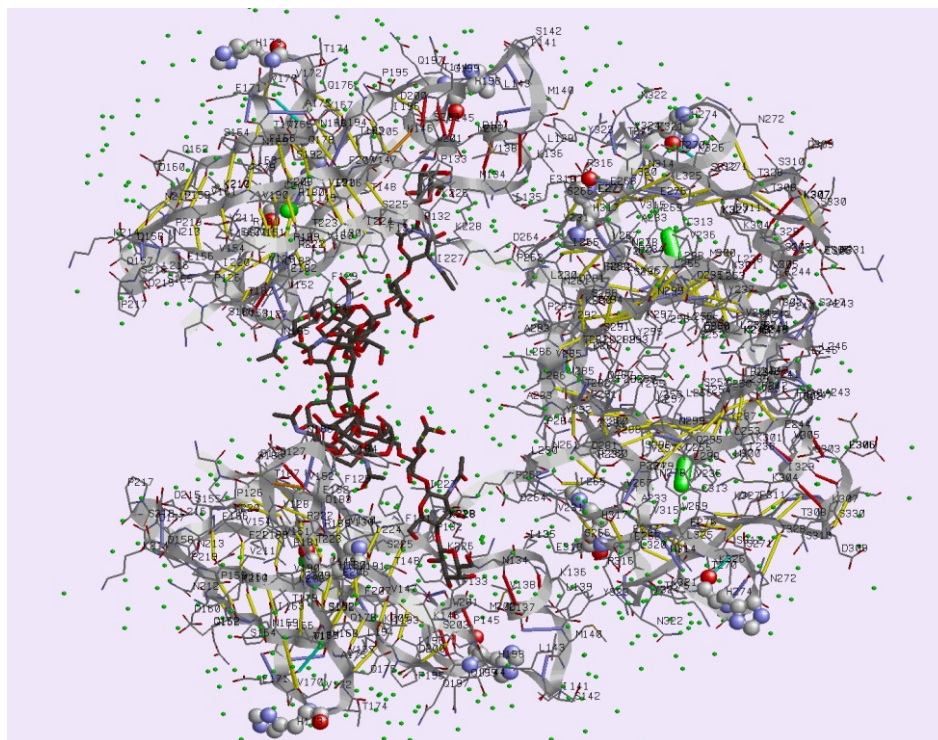


**Fig. 1.** Schematic view of the Fc fragment of mouse immunoglobulin IgG2b. Each of the protein chains A,B (upper and lower) divides into two compact domains C 2 (loosely joined together by non-covalent interactions of oligosaccharide chains [black lines] - left side) and more compact dimer of two C 3 domains (right side). Small spheres are water molecules in positions stabilized by hydrogen bridges to the molecular complex.

The oligosaccharide chains joining the two protein chains were taken from the protein structure database PDB /8/ - the structure of immunoglobulin IgG2a (PDB code 1I1C). Both chains -NAG<sub>1</sub>(FUC)-NAG<sub>2</sub>-MAN<sub>3</sub>(MAN-NAG-GAL)-MAN<sub>4</sub>-NAG<sub>5</sub> are chemically bound to Fc fragment through asparagines Asn185A and Asn185B. The MAN-NAG-GAL branch of both oligosaccharide chains has contacts to its own protein chain only. The chains -MAN<sub>3</sub>-MAN<sub>4</sub>-NAG<sub>5</sub> of both Fc fragment halves form several hydrogen bonds joining thus both CH2 domains together.

### Conclusion

A detailed structure of the intact Fc fragment of IgG2b in buffer with pH 7.5 determined in this paper is important for elucidation of the structure changes and the interactions with proteins possessing high selectivity for Fc fragment surface. These include complement components responsible for immunological response, viral proteins (protein A, protein G,...), cell surface receptors and specially designed molecules suitable for highly efficient separation of immunoglobulines by affinity chromatography.

*The project is supported by MSMT - 1K05008.*

### References

- Otwinowski Z. & Minor, W. (1997). Processing of X-ray diffraction data collected in oscillation mode. *Methods Enzym.*, **276**, 307-326.
- Navaza, J. Saludjian, P. (1994). AMoRe: An automated molecular replacement program package. *Acta Crystallog. Sect. A*, **50**, 157-163.
- Collaborative Computational Project, Number 4 (1994). The CCP4 Suite: Programs for Protein Crystallography. *Acta Crystallog. Sect. D*, **50**, 760-763.
- Murshudov, G. N., Vagin, A. A. Dodson, E. J. (1997). Refinement of Macromolecular Structures by the Maximum-Likelihood Method. *Acta Crystallog. Sect. D*, **53**, 240-255.
- McRee, D. E. (1999). XtalView/Xfit - A Versatile Program for Manipulating Atomic Coordinates and Electron Density. *J. Struct. Biol.*, **125**, 156-165.
- Perrakis, A., Harkiolaki, M., Wilson, K.S. & Lamzin, V.S. (2001). ARP/wARP and molecular replacement. *Acta Crystallog. Sect. D*, **57**, 1445-1450.
- Laskowski, R. A., MacArthur, M. W., Moss, D. S. Thornton, J. M. (1993). Procheck - a program to check the stereochemical quality of protein structures. *J. App. Cryst.* **26**, 283-291.
- H.M. Berman, J. Westbrook, Z. Feng, G. Gilliland, T.N. Bhat, H. Weissig, I.N. Shindyalov, P.E. Bourne: The Protein Data Bank. *Nucleic Acids Research*, **28** pp. 235-242 (2000).
- Petroková, H., Vondráčková, E., Skálová, T., Dohnálek, J., Lipovová, P., Spiwok, V., Strnad, H., Králová B. Hašek, J. (2005). Crystallization and preliminary X-ray diffraction analysis of cold-active  $\beta$ -galactosidase from *Arthrobacter* sp. C2-2. *Collect. Czech. Chem. C.*, **70**, 124-132.



S16

## INSIGHT INTO STRUCTURE - FUNCTION RELATIONSHIPS OF *RALSTONIA SOLANACEARUM* LECTINS RSL, RS-IIL AND RS20L

Nikola Kostlánová<sup>1</sup>, Edward P. Mitchell<sup>2</sup>, Nechama Gilboa-Garber<sup>3</sup>, Michaela Wimmerová<sup>1</sup> and Anne Imberty<sup>4</sup>

<sup>1</sup>National Centre for Biomolecular Research and Department of Biochemistry, Masaryk University, Kotlářská 2, 61137 Brno, Czech Republic, <sup>2</sup>E.S.R.F. Experiments Division, BP 220, F-38043, Grenoble Cedex, France,

<sup>3</sup>Faculty of Life Sciences, Bar-Ilan University, Ramat-Gan 52900, Israel,

<sup>4</sup>CERMAV-CNRS, BP 53, F-38041, Grenoble, Cedex 09, France

Lectins are a class of proteins of non-immune and non-enzymatic origin that bind carbohydrates specifically and reversibly. They express numerous biological activities, nearly all of which are based on their acting as recognition determinants in diverse biological processes including fertilization, pathogen-cell adhesion and recognition, inflammatory response and others. A number of pathogen microorganisms utilize lectin-carbohydrate interaction to recognize and infect host organism. The comprehension of the molecular mechanisms which gives a pathogenic bacterium the ability to invade, colonize and reorient the physiopathology of its host is a goal of primary importance and such studies may direct the conception of new strategies to fight these pathogenic agents 1 .

*Ralstonia solanacearum* is soil-born bacterium, which belongs to the group of beta-proteobacteria. It is responsible for bacterial wilts on more than 200 plant species including potato, tomato banana and others economically important crops 1 . *R. solanacearum*, which is capable of living for prolonged periods in the soil, infects its hosts beginning with the root system and presents a very strong tropism for the xylem vessels. Its extensive multiplication in the water-conducting system leads to a systemic infection of the plant.

This contribution describes three lectins RSL (9.9 kDa) 2 , RS-IIL (11.6 kDa) 3 and RS20L (20 kDa) that have

been found in *R. solanacearum* extract and purified using affinity chromatography. All lectins were crystallized by vapor diffusion and high and ultra-high (in case of 0.94 Å resolution of RSL/ -methylfucoside) resolution data were collected at ESRF, Grenoble, France. The structural data have been supplemented by ITC microcalorimetry and surface plasmon resonance studies defining lectins specificity to carbohydrates including those, which are commonly present in nature and may be the target for the lectins in plants.

- 1 Salanoubat, M., Genin, S., Artiguenave, F., Gouzy, J., Mangenot, S., Arlat, M., Billault, A., Brottier, P., Camus, J.C., Cattolico, L., Chandler, M., Choisine, N., Claudel-Renard, C., Cunnac, S., Demange, N., Gaspin, C., Lavie, M., Moisan, A., Robert, C., Saurin, W., Schiex, T., Siguier, P., Thebault, P., Whalen, M., Wincker, P., Levy, M., Weissenbach, J. & Boucher, C.A., *Nature*, 415 (2002) 497-502.
- 2 Kostlánová, N., Mitchell, E., Lortat-Jacob, H., Oscarson, S., Lahmann, M., Gilboa-Garber, N., Chambat, G., Wimmerová, M., & Imberty, A., *J Biol Chem*, in press.
- 3 Sudakevitz, D., Kostlánová, N., Blatman-Jan, G., Mitchell, E., Lerrer, B., Wimmerová, M., Katcoff, D.J., Imberty, A. & Gilboa-Garber, N., *Mol. Microbiol.*, 52(3) (2004), 691-700.

S17

## CRYSTAL STRUCTURE OF CV-IIL LECTIN FROM HUMAN OPPORTUNISTIC PATHOGEN

M. Pokorná<sup>1</sup>, G. Cioci<sup>2</sup>, E. P. Mitchell<sup>3</sup>, S. Perret<sup>2</sup>, A. Imberty<sup>2</sup> and M. Wimmerová<sup>1,4</sup>

<sup>1</sup>National Centre for Biomolecular Research, Masaryk University, Kotlářská 2, 611 37 Brno, Czech Republic

<sup>2</sup>CERMAV-CNRS, 601 rue de la Chimie, BP 53, 38041 Grenoble, France

<sup>3</sup>ESRF, Experiments Division, BP 220, 38043 Grenoble, France

<sup>4</sup>Department of Biochemistry, Masaryk University, Kotlářská 2, 611 37 Brno, Czech Republic

Carbohydrates are essential components of life that play crucial role in all organisms. They are very important agent in recognition and signalling ways. Lectin-carbohydrate interactions play a crucial role in many recognition events.

*Chromobacterium violaceum* is a gram-negative bacterium first described at the end of 19<sup>th</sup> century. This bacterium has been found in tropical and subtropical regions, water and borders of the Negro river. *Ch. violaceum* is an

opportunistic pathogen and may cause diseases in immunocompromised individuals [1]. It is phylogenetically related with human pathogen *Pseudomonas aeruginosa*, which produces PA-IIL lectin, closely related with its virulence.

The contribution is focused on identification and structure-function characterisation of PA-IIL homolog, CV-IIL,



found by searching in sequenced bacterial genome of *Ch. violaceum* [2]

The gene of the protein has been cloned and resulting protein CV-IIL has been purified by affinity chromatography. CV-IIL/ -methyl-D-mannoside and CV-IIL/ -methyl-L-fucoside complexes have been crystallised by hanging drop vapor diffusion method using high-molecular weight PEGs as precipitants. Diffraction data at 1.0 Å resolution were collected under cryogenic conditions (100K) on the beamline ID14-2, at ESRF, Grenoble, France. The crystal structures of CV-IIL in complexes with sugar ligands were solved by molecular replacement.

Structure studies together with binding data analysis allowed comparison of CV-IIL and PA-IIL and brought more detailed view on fine specificity of both lectins.

- [1] Ribeiro De Vasconcelos, A.T. & 109 others [Brazilian National Genome Project Consortium]; The complete genome sequence of *Chromobacterium violaceum* reveals remarkable and exploitable bacterial adaptability. Proc. Natl. Acad. Sci. **100**, 11660 (2003).
- [2] Imberty A, Wimmerová M, Mitchell E.P., Gilboa-Garber, N. Structures of the lectins from *Pseudomonas aeruginosa*: Insights into molecular basis for host glycan recognition. Microb. Infect. **6**: 222-229 (2004).

**S18**

## MAS NMR A RTG STUDIE ZEOLITIZACE KOMPOZITŮ SLOŽENÍ POPÍLEK-METAKAOLIN (KAOLIN) - NaOH V HYDROTERMÁLNÍCH PODMÍNKÁCH

M. Urbanová<sup>1</sup>, J. Brus<sup>1</sup>, D. Koloušek<sup>2</sup>

<sup>1</sup>Ústav makromolekulární chemie AV ČR, Heyrovského náměstí 2, Praha 6;

<sup>2</sup>VŠCHT, Technická 5, Praha 6) E-mail: [urbanova@imc.cas.cz](mailto:urbanova@imc.cas.cz)

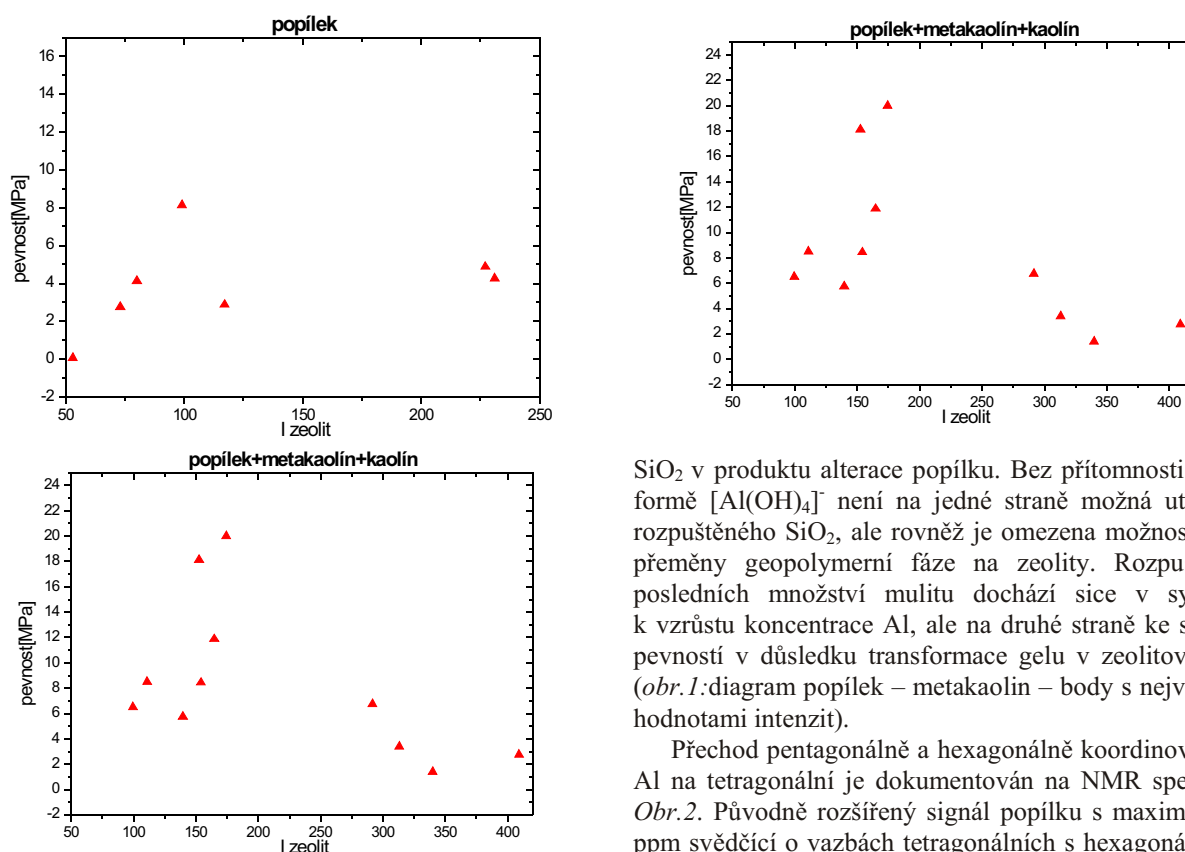
Popílký se vyznačují vysokou hydraulickou aktivitou. Způsoby alkalických aktivací prováděné při laboratorních teplotách jsou známé. Jde především o klasické zpevňování na bázi pucolánických reakcí. V poslední době se objevují reference o vzniku geopolymerních gelů v systémech popílek – Na-vodní sklo. Geopolymerní reakce vyžadují přítomnost rozpuštěných forem SiO<sub>2</sub>, jejichž potřebu saturuje právě přídavek vodního skla. Forma Al<sup>3+</sup> do reakce vstupuje především z amorfních složek popílku a méně pravděpodobně z mulitu (3Al<sub>2</sub>O<sub>3</sub>·2SiO<sub>2</sub>). Majoritní složkou popílku je křemen, jehož rozpustnost stoupá se stoupajícím pH a teplotou. Záměrem této práce bylo využití rozpouštění křemene, mulitu a amorfních složek při vývoji geopolymerních reakcí v systémech aktivovaných NaOH v hydrotermálních podmínkách a také jakým způsobem ovlivňuje přídavek metakaolinu eventuelně ve směsi s kaolinitem do tohoto systému dosažené pevnosti.

Pro dosažení tohoto cíle byly připravovány kompozity obsahující 50 g popílku (Teplárna Strakonice) nebo 30 g popílku + 20 g metakaolinu. Kompozity byly rovněž připraveny ze směsi 30g popílku + 20 g částečně žíhaného kaolinu (v produktu žíhání bylo zjištěno cca 30% původního obsahu kaolinitu). Alkalická aktivace tohoto systému byla provedena 31g 10M roztoku NaOH. Ze směsi byly vytvářeny kostičky (2x2x2 cm), které byly temperovaly při 80°C po dobu 5 hodin nejdříve zabalené ve folii a 5 hodin uloženy volně v sušárně při téže teplotě. Kostičky byly po dobu 1 týdne uloženy v exsikatoru a poté byly podrobeny hydrotermální aktivaci v autoklávech při izotermách 100, 140 a 180°C po dobu 24 hodin v bezvodém prostředí a v přídávku 10 ml H<sub>2</sub>O. Při stejných teplotách byly provedeny experimenty v autoklávech s expozicí 168 hodin v prostředí H<sub>2</sub>O. Ihned po vyjmutí z autoklávů byly kostičky podrobeny měření pevnosti v tlaku. Z každé řady experimentů rezultovalo 11 výsledků pevnostních měření (9 autoklávovaných kompozitů a 2 z normálního zrání po 7 a 90 dnech). Korelace dosažených

pevností byla prováděna na základě kvantitativního parametru vycházející z rtg. práškové difrakce charakterizující vznik sekundárních složek (především zeolitů) a úbytku zdrojových složek – křemene a mulitu v kompozitech. Některé produkty byly rovněž podrobeny analýze MAS NMR.

Dosažené pevnosti v tlaku kompozitů nekorrespondují s teplotními a časovými expozicemi hydrotermálního působení. V silně alkalickém prostředí dochází k aktivaci systému rozpouštěním amorfních a krystalických složek (v případě popílku křemene a při vyšších teplotách rovněž mulitu). Kompozity připravené pouze z popílku při alkalické aktivaci dosahovaly pevnosti maximálně do 10 MPa. Vyšší pevnosti při srovnatelných podmínkách přípravy a teplotního zpracování byly zjištěny v systému metakaolin - popílek - NaOH a nejvyšší (až 27MPa) v systému metakaolin (kaolin) - popílek – NaOH. Pevnosti v tlaku kompozitů se zvyšují s rostoucím obsahem zeolitových fází. Závislosti nejsou nikterak ostré, protože se pevnosti mohou lišit u stejně připravených kompozitů o jednotky MPa. Trendy jsou však zřejmé (viz Obr.1). Se vzrůstajícím obsahem zeolitových fází se rovněž zvyšuje odolnost vůči tlaku. Určitou výjimkou jsou experimenty systému metakaolin – popílek – NaOH, kdy došlo k rozsáhlé rekrystalizaci materiálu provázené snížením pevnosti neodpovídající naznačenému trendu. Tuto závislost je možno korelovat vymizením charakteristických reflexí mulitu z rentgenového záznamu a výrazným vzrůstem intenzit zeolitových minerálů (konkrétně analcimu).

Vývoj pevností je především ovlivněn přítomností amorfních složek v popílku. V tomto kontextu bývají popisované sklovité fáze či pozůstatky metakaolinu tepelně nepřeměněného do mulitické složky. Sklovité složky jsou reaktivní a s největší pravděpodobností vytváří svým rozpouštěním gel geopolymerního typu, který má výrazný podíl na růstu pevnosti kompozitů podrobených normálnímu zrání. Se vzrůstající teplotou dochází k akceleraci



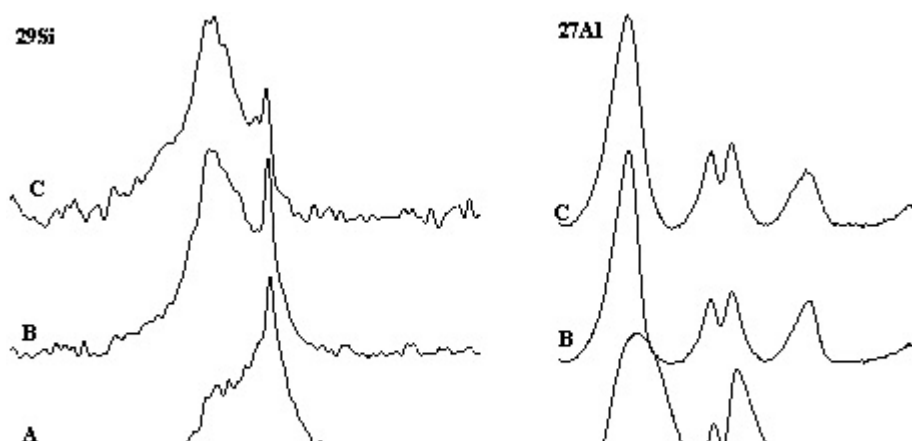
**Obr. 1.** Závislost intenzit vybraných úseků rtg difrakčního práškového záznamu charakterizující přítomnost zeolitů na dosažené pevnosti kompozitů v jednotlivých systémech.

rozpuštění amorfních složek ale také křemene obsaženého v popílku. Rozpuštěné formy  $\text{SiO}_2$  reagují s metakaolinem za vzniku geopolymerní sítě a zároveň dochází ke vzniku zeolitových fází v této matici. Tato reakční fáze je charakterizována nárůstem mechanických pevností, který je možno korelovat úbytkem křemene a snad mulitu a vrůstajícím množstvím zeolitových fází v systému (tento úbytek je nejen detekovatelný na rtg záznamu, ale i na NMR spektrech obrázku 2 v oblasti  $-107\text{ppm}$  úbytkem intenzity). Schopnost systému dodávat zdrojové složky pro výstavbu geopolymerní sítě není neomezená, protože dostupné formy Al se vyčerpají. NMR spektra (Obr.2) dokládají přítomnost monomerních forem

$\text{SiO}_2$  v produktu alterace popílku. Bez přítomnosti Al ve formě  $[\text{Al}(\text{OH})_4]$  není na jedné straně možná utilizace rozpuštěného  $\text{SiO}_2$ , ale rovněž je omezena možnost další přeměny geopolymerní fáze na zeolity. Rozpuštěním posledních množství mulitu dochází sice v systému k vzrůstu koncentrace Al, ale na druhé straně ke snížení pevností v důsledku transformace gelu v zeolitové fáze (obr.1: diagram popílek – metakaolín – body s nejvyššími hodnotami intenzit).

Přechod pentagonálně a hexagonálně koordinovaného Al na tetragonální je dokumentován na NMR spektrech Obr.2. Původně rozšířený signál popílku s maximem 56 ppm svědčící o vazbách tetragonálních s hexagonálním a pentagonálním Al, se postupně zužuje tak, jak se vytváří geopolymerní sítě. Pentagonálně koordinovaný Al přetrvává v produktech jako mulit.

Experimentální práce prováděné v autoklávech se vyznačují tím, že je možno získat jen velmi málo informací o přechodných stádiích probíhajících během hydrotermálního procesu. Prášková difrakční analýza vede k základním informacím o produktech, ale vzhledem ke své fyzikální podstatě nemůže vysvětlit mechanismy jejich vzniku. MAS NMR podává právě o těchto procesech neocenitelné údaje a z tohoto hlediska je důležitou komplementární metodou k rtg. analýze.



**Obr. 2.** Spektra  $^{29}\text{Si}$  a  $^{27}\text{Al}$  pro vzorky A – popílek Strakonice; B – popílek + 10M NaOH po 7 denním zrání (dosažená pevnost v tlaku 5MPa), C – popílek + 10M NaOH po hydrotermálním zpracování při  $180^\circ\text{C}$  (24h, 9MPa).

## STEREOCHEMISTRY OF CALIX[4]ARENES

J. Klimentová and P. Vojtíšek

Department of Inorganic Chemistry, Faculty of Science, Charles University, Prague, Czech Republic

Calix[4]arenes are a fascinating class of macrocyclic compounds, which has recently attracted a lot of attention because of their potential wide use in many areas of research and industry. Having started in the 19<sup>th</sup> century by reactions of phenol and aldehydes performed by Adolph von Baeyer; and continued by a considerable effort of David C. Gutsche in the 1970s, the chemistry of calixarenes has developed into a wide and well-explored area [1]. Calix[4]arenes have been used principally as spacers bearing functional groups in a well-defined arrangement, allowing their desired cooperation [2].

The utilization of calixarenes as molecular platforms possesses a few advantages. First, the synthesis of these macrocycles can be easily accomplished by a well-known procedure in good yields. The size of the macrocycle can be successfully controlled by the reaction conditions [3]. The starting materials (*p-tert*.butylphenol and formaldehyde) are inexpensive and common. Calix[4]arenes can be easily modified both on their upper and lower rim [3], which allows to change their chemical and physical properties as required. Finally, the four possible conformations of the calix[4]arene macrocycle, easily immobilized by lower-rim substitution [2], are the main reason for the advantage of using calix[4]arenes as molecular platforms.

Recently, heterocalix[4]arene macrocycles have been synthesized. These compounds contain a heteroatom (S, N, Si) or a functional group based on heteroatom (SO, SO<sub>2</sub>) instead of the methylene bridge, which is responsible for their greater conformational flexibility [4].

The conformation and symmetry of the calix[4]arene molecule is important for its function as a spacer bearing substituents in a defined arrangement, which allows their interaction, interaction with cations, anions or neutral molecules, cooperation in ion pair binding etc. [2, 5]. Another important factor is the rigidity or flexibility of the substituents and of the calix[4]arene skeleton. The rigidity of the latter can be achieved by bridging the upper or lower rim of the calix[4]arene molecule, effectively locking its movements [2]. Furthermore, the conformation of the calix[4]arene platform can be influenced by the interactions of its hydrophobic cavity or aromatic rings with cations or neutral molecules by the means of cation-interactions,  $\pi$ -interactions or van der Waals interactions. The substituents on the upper or lower rim may also participate in shaping of the calix[4]arene molecule. The possible interactions (beside the above mentioned ones) may involve inter- or intramolecular hydrogen bonding, electrostatic interactions, donor-acceptor interactions (cation complexes or Lewis acid-base pairing) and sterical hindrance. In conclusion, the final shape of the calix[4]arene platform results from the combination of all these effects.

To elucidate the influence of the substitution on the upper and lower rim of the calix[4]arene and inter- or

the angle of the phenyl ring to the reference plane

the reference plane of the methylene groups

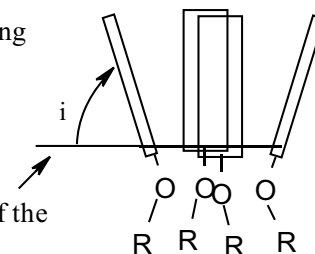


Fig. I. The definition of the phenyl ring angles  $\phi_i$ .

intramolecular interactions on the conformation of the calix[4]arene molecule, we decided for the Cambridge Structural Database [6] as the largest source of information (about 1,500 calix[4]arene structures). The conformation of the calix[4]arene molecules and inter- or intramolecular interactions of these compounds can be easily determined from the crystal structure data. Nevertheless, this information might not fully correspond to the conformational behavior of the calix[4]arene molecules in solution.

To describe the conformation of the calix[4]arene skeleton, a variety of geometrical parameters can be calculated (e.g. the distances between the oxygen or carbon atoms on the lower or upper rim, the angles of the planes of the phenyl rings etc.). We have decided to describe the calix[4]arene conformation by the defining of a reference plane to which the angles of the four phenyl rings are related. The most convenient reference plane appears to be the plane of the four methylene bridging groups (for the vast majority of structures, the deviation of the methylene carbon atoms from this plane is below 0.01 nm). The angles of the phenyl rings ( $\phi_i$ ,  $i = 1-4$ ) are calculated in the scale 0-360 (see Fig. I).

Next step in the description of the calix[4]arene conformations is the definition of geometrical parameters  $\bar{\phi}$ ,  $\delta$ , according to (1).

$$0.25(\phi_1 + \phi_2 + \phi_3 + \phi_4) \quad (1)$$

The parameter  $\bar{\phi}$  is the average value of the phenyl ring angles  $\phi_1 - \phi_4$  (numbering reflects the order of the phenyl rings in the calix[4]arene molecule, e.g.  $\phi_1, \phi_2$  corresponds to adjacent rings,  $\phi_1, \phi_3$  to opposite rings etc.). The parameter  $\delta$  reflects the distortion of the calix[4]arene molecule towards  $C_{2v}$  symmetry (for calix[4]arenes in the *cone* conformation). Finally,  $\sigma$  reflects the distortion towards  $C_s$  symmetry (again, for calix[4]arenes in the *cone* conformation). Further examples of the dependence of the parameters  $\bar{\phi}$ ,  $\delta$ ,  $\sigma$  on the calix[4]arene conformation are depicted in Fig. II (the schemes show slices through the calix[4]arene opposite rings and usual angles).

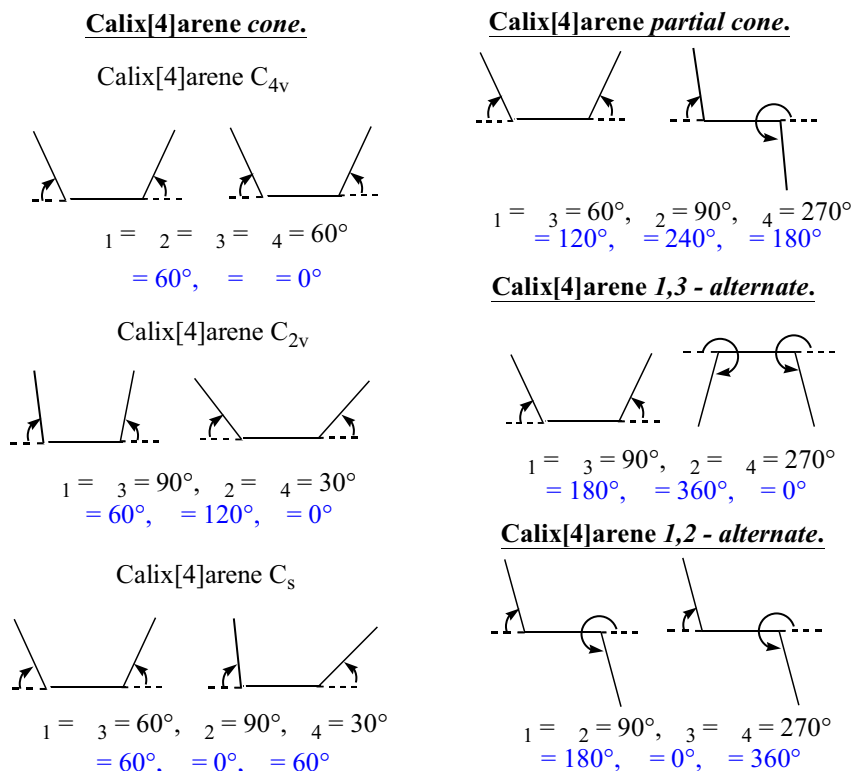


Fig. II : Parameters , , in dependence on the calix[4]arene conformation and symmetry.

The parameters  $\alpha, \beta$  reflect the conformation of the calix[4]arene molecules (see Fig. II) For example, all calix[4]arenes in the *cone* conformation have  $\alpha < 90^\circ$  and the values of  $\beta, \gamma$  reflect their distortion towards  $C_{2v}, C_s$  or  $C_1$  symmetry (the latter for both  $\beta, \gamma$  significantly different from zero). The dependence of the  $\alpha, \beta, \gamma$  values is shown on the group of heterocalix[4]arenes in Fig. III.

The dependence of the parameters  $\alpha, \beta, \gamma$  on the symmetry of the calix[4]arene is shown on the example of non-complexed calix[4]arenes in the *cone* conformation symmetrically tetrasubstituted on the upper and lower rim (Fig. IV).

The deformation of the symmetrically tetrasubstituted *cone*-calix[4]arene molecules towards  $C_{2v}, C_s$  or  $C_1$  sym-

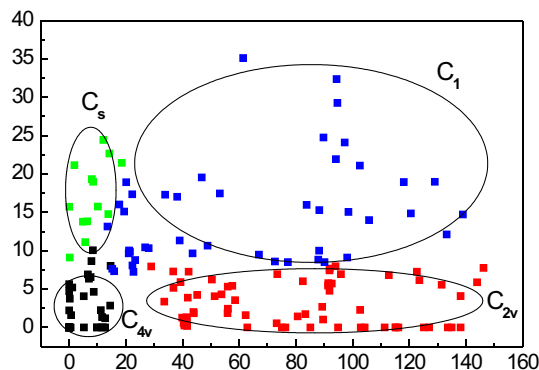


Fig. IV. The dependence of the parameters  $\alpha, \beta, \gamma$  on the symmetry of the symmetrically tetrasubstituted *cone*-calix[4]arenes not bound to metal from [6].

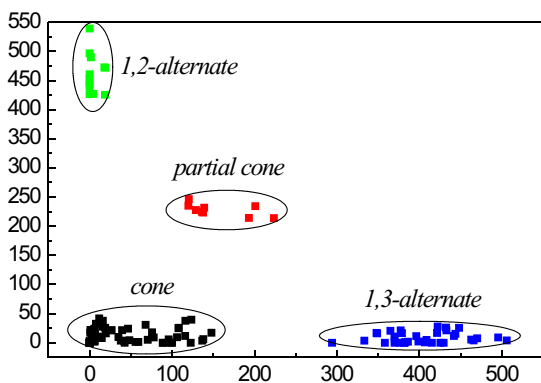


Fig. III. The distribution of the  $\alpha, \beta, \gamma$  values in the group of heterocalix[4]arenes from [6].

metry is caused by the above-mentioned types of interactions, principally cation complexation,  $\pi$ -stacking, hydrogen bonding and sterical hindrance. Some examples are given on Fig. V.

The dependence of the calix[4]arene symmetry on changing the substitution pattern of the upper or lower rim can be also considered. Nevertheless, the dependence is complex and results from the combination of sterical and electronic effects. Our further attempts on this field are in progress.

Due to the large amount of CSD data and limited space in this abstract, only a few examples of the influence of the interactions on the shape of the calix[4]arene molecule are presented.



- [1] C.D. Gutsche, *Calixarenes*, Monographs in Supramolecular Chemistry, The Royal Society of Chemistry, J.F. Stoddart, Cambridge 1989.
- [2] S. Shinkai, A. Ikeda, *Chem. Rev.*, **97** (1997), 1713-1734.
- [3] *Macrocyclic Synthesis*, editor D. Parker, Oxford University Press, New York 1996.
- [4] P. Lhoták, *Eur. J. Org. Chem.*, (2004), 1675-1692.
- [5] P.D. Beer, P. Gale, *Angew. Chem. Int. Ed.*, **40** (2001), 486-516.
- [6] CSD, Cambridge Crystallographic Data Centre (CCDC).

S20

### TANTALONIOBATES IN CASSITERITE: INCLUSIONS OR EXOLUTIONS?

M. Klementová<sup>1,2</sup>, M. Rieder<sup>3</sup>

<sup>1</sup>*Institute of Inorganic Chemistry, Academy of Sciences of the Czech Republic*

<sup>2</sup>*IGMMR, Faculty of Science, Charles University in Prague, Czech Republic*

<sup>3</sup>*Institute of Materials Chemistry, VŠB – Technical University of Ostrava*

See page 104.

S21

### CRYSTALLOGRAPHY OF THE Sb-Te-Ni SYSTEM

F. Laufek<sup>1,3</sup>, M. Drábek<sup>1</sup>, R. Skála<sup>2</sup>, I. Čísařová<sup>3</sup>

<sup>1</sup>*Czech Geological Survey, Geologická 6, Praha 5, 152 00, Czech Republic*

<sup>2</sup>*Institute of Geology, Academy of Sciences of the Czech Republic, Rozvojová 135, Praha 6, 165 02*

<sup>3</sup>*Faculty of Science, Charles University, Hlavova 8, , Praha 2, 128 43, Czech Republic*

The new unnamed nickel antimonide telluride Ni<sub>2</sub>SbTe<sub>2</sub> was found as 6 m grain by Vavřín and Frýda [1] at the Kunratice Cu-Ni deposit (North Bohemia). This ternary phase is in a close association with melonite (NiTe<sub>2</sub>); this assembly is included in pyrrhotite (Fe<sub>1-x</sub>S). In order to determine the crystal structure of this phase (from the synthetic analogue) and to further explore the Ni-Sb-Te phase diagram, the crystallography of this ternary system was investigated. The phases were prepared using the silica glass tube method. Our experiments were performed in the Experimental laboratory of Czech Geological Survey. High-purity elements – tellurium (99.999 %), antimony (99.99 %) and nickel (99.995 %) were used as starting materials. Before being used for syntheses, nickel was heated for 1 hour in a stream of H<sub>2</sub> at 800 °C. Carefully weighted samples were loaded into the high purity silica tubes and tightly fitting silica rods were placed on the top of the reagents in order to reduce the vapour volume during heating. The silica tubes with the charge were sealed under vacuum and

then heated in the horizontal furnaces in which the temperature was controlled electronically. The maximum temperature variation did not exceed 4 °C. The samples were heated at 400°C or at 800°C for three weeks. The experiments were terminated either by quenching in a cold bath or by slow controlled cooling to room temperature.

The crystal structure of the new phase Ni<sub>2</sub>SbTe<sub>2</sub> prepared at 800°C (experiment terminated by quenching), determined from X-ray single diffraction data, is hexagonal, NiAs type, with lattice parameters:  $a = 3.9108(2)$ ,  $c = 5.2489(3)$  Å, space group  $P6_3/mmc$  (no. 194). The antimony and tellurium occupy the crystallographic position  $2c$ ; the position  $2a$  is occupied by nickel atoms (Fig. 1)

The crystal structure of Ni<sub>2</sub>SbTe<sub>2</sub> prepared at 400 °C (experiment terminated by slow controlled cooling to room temperature within interval 22 hours), originally described by [2], refined from single X-ray diffraction data, is hexagonal with lattice parameters  $a = 3.9110(2)$ ,  $c = 15.696(1)$

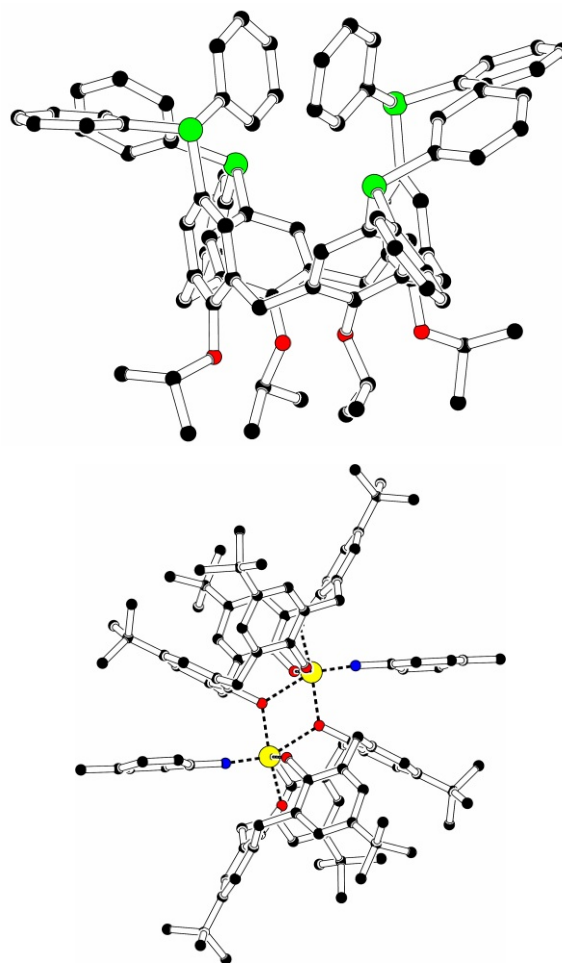
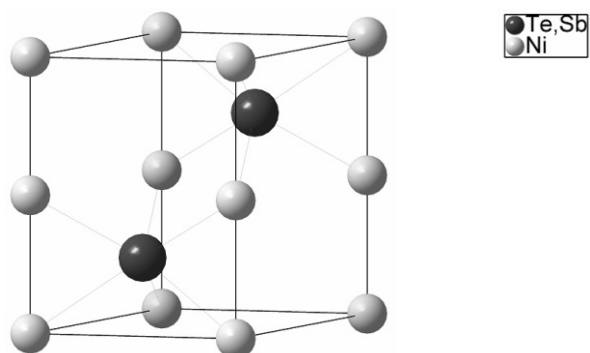


Fig. V. Examples of deformation of the calix[4]arene molecule towards C<sub>2v</sub> and C<sub>s</sub> symmetry (atom colors : black C, red O, blue N, green P, yellow W) [6].





**Fig. 1.** Crystal structure of  $\text{Ni}_2\text{SbTe}_2$  prepared at  $800^\circ\text{C}$  (experiment terminated by quenching).

$\text{Å}$ , space group  $P6_3/mmc$  (no. 194). The antimony and tellurium atoms occupy different crystallographic positions, antimony  $2c$  and tellurium  $4f$ . (Fig. 2). The crystal structure can be described as “hybrid” of  $\text{NiSb}$  and  $\text{NiTe}_2$  with an elongated  $c$ -axis. In  $\text{NiSb}$  structure, the close packed anion layers are all  $\text{Sb}$  with  $\text{ABAB}$  stacking and all octahedral holes are filled with  $\text{Ni}$ . If every third plane of  $\text{Ni}$  atoms is removed from  $\text{NiSb}$  and  $\text{Sb}$  replaced with  $\text{Te}$  in two out of three layers, we can obtain the  $\text{Ni}_2\text{SbTe}_2$  structure (low temperature modification). The atom stacking sequence is  $\text{CABCAC}$  ( $\text{A} - \text{Ni}$ ,  $\text{B} - \text{Sb}$ ,  $\text{C} - \text{Te}$ ). The interlayer  $\text{Te} - \text{Te}$  distance is  $3.543 \text{ Å}$ . It is also to be noted that this interatomic distance is larger than  $\text{Te}_2$  pair-containing phases ( $2.763 \text{ Å}$  in  $\text{HfTe}_2$  and  $2.793 \text{ Å}$  in  $\text{ZrTe}_2$ ) or in elementary  $\text{Te}$  ( $2.84 \text{ Å}$ ) [3], but shorter than the van der Waals distance  $4.12 \text{ Å}$  (default van der Waals radius for  $\text{Te}$  is taken from [4]). The weak interlayer  $\text{Te}$  bonding results in a layered structure which corresponds to plate-like morphology of crystals.

The situation in the case of crystal structure of  $\text{Ni}_2\text{SbTe}_2$  prepared at  $400^\circ\text{C}$  (experiment terminated by quenching) is more complicated. The X-ray powder diffraction pattern corresponds to the high temperature phase, nevertheless diffraction profiles of  $201$  and  $110$  lines are asymmetrical. This asymmetry disappears in the powder pattern of  $\text{Ni}_2\text{SbTe}_2$  prepared at  $800^\circ\text{C}$  (experiment terminated by quenching, Fig. 3). On the Selected Area Electron Diffraction (SAED) pattern of reciprocal planes  $h0l$  it is

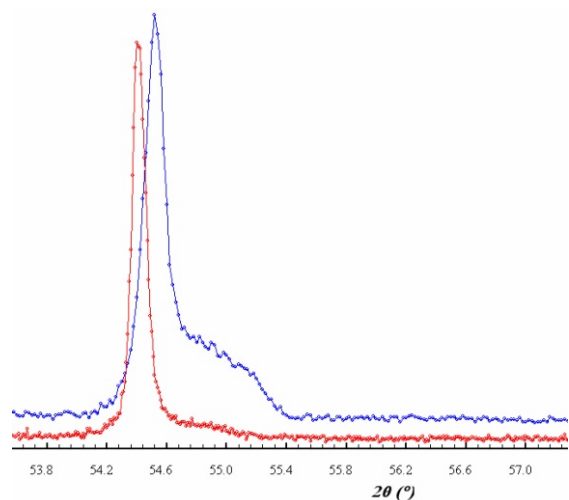


**Fig. 3.** Diffraction profile of  $110$  line of  $\text{Ni}_2\text{SbTe}_2$  prepared at  $400^\circ\text{C}$  (above) and at  $800^\circ\text{C}$ ,  $\text{CoK } \alpha_1$ .

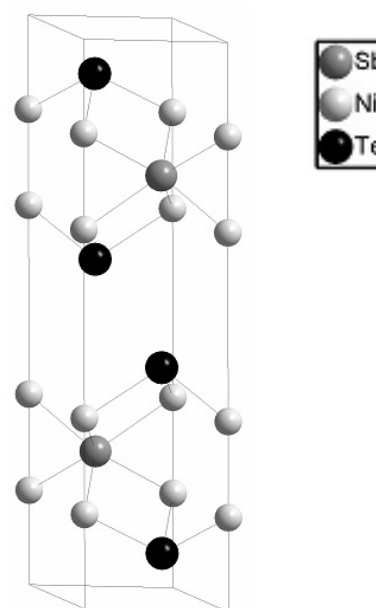


**Fig. 2.** Crystal structure of  $\text{Ni}_2\text{SbTe}_2$  prepared at  $400^\circ\text{C}$  (experiment terminated by slowly cooling to room temperature).

possible to observe weak reflections near  $1/3$  and  $2/3$  of the distance between the sharp strong diffractions. These weak reflections are systematically shifted from  $1/3$  to the left and from  $2/3$  to the right, i.e. closer to the sharp strong diffraction.

In fact, there is a large number of compounds that exhibit  $\text{Sb} - \text{Te}$  bonding in which  $\text{Sb}$  is formally cationic. Examples of such compounds include  $\text{K}_3\text{SbTe}_3$ ,  $\text{TlSbTe}_2$ ,  $\text{SnSb}_2\text{Te}_4$ ,  $\text{BaSbTe}_3$  and  $\text{NaSbTe}_2$  [2]. In many compounds the  $\text{Sb}$  and  $\text{Te}$  atoms are mixed on the same crystallographic site and thus are not new structure types. These include e.g.  $\text{Ni}_2\text{SbTe}$ ,  $\text{Mn}_2\text{SbTe}$ ,  $\text{Co}_2\text{SbTe}$ ,  $\text{FeSbTe}$ ,  $\text{Pd}_2\text{SbTe}$  and  $\text{Cr}_2\text{SbTe}$  [5]. Virtually, there are very few compounds which have  $\text{Sb}$  and  $\text{Te}$  atoms on distinct crystallographic positions. Examples of such compounds are  $\text{Ni}_{7-8}\text{SbTe}_2$ ,  $\text{Cu}_{9,1}\text{Sb}_3\text{Te}$  and the new compound  $\text{Ni}_2\text{SbTe}_2$ . Our research showed that the crystal structure of this phase depends on the temperature during the formation.

The phase  $\text{Ni}_2\text{SbTe}_2$  forms a solid solution with end members having a composition of  $42,1 \%$   $\text{Ni}$ ,  $13,0 \%$   $\text{Sb}$ ,  $44,9 \%$   $\text{Te}$  and  $43,0 \%$   $\text{Ni}$ ,  $28,4 \%$   $\text{Sb}$ ,  $28,6 \%$   $\text{Te}$  (at.%) at  $400^\circ\text{C}$ . The most characteristic feature is a small change of the nickel content as well as significant differences of the antimony and tellurium content

*This work was supported by a Grant Agency of Charles University (project number 43-203391).*

1. Vavřín, I. & Frýda, J. *Věstník ČGÚ*, **73** (1998) 177-180.
2. Reynolds T.K., Kelley R.F. & DiSalvo F.J. *J. Alloy Comp.*, **366** (2004) 136 -144.
3. Bensch, W., Heid, W., Muhler, M., Jobic, S., Brec, R. & Rouxel, J. *J. Solid State Chem.* **121** (1996) 87 - 94.
4. Bondi, A. *J. Phys. Chem.* **68** (1964) 441-451.
5. Inorganic Crystal Structure Database (ICSD), 2003